CDDpress

www.nature.com/cddis

ARTICLE OPEN

S-nitrosylation of CSF1 receptor increases the efficacy of CSF1R blockage against prostate cancer

Fakiha Firdaus[1,6], Manish Kuchakulla[1,6], Rehana Qureshi[2,6], Raul Ariel Dulce[3], Yash Soni[1], Derek J. Van Booven[2], Khushi Shah[1], Thomas Masterson[1], Omar Joel Rosete[1], Sanoj Punnen[1], Joshua M. Hare[2,3,4,5], Ranjith Ramasamy[1,3] and Himanshu Arora[1,2,3]✉

Sustained oxidative stress in castration-resistant prostate cancer (CRPC) cells potentiates the overall tumor microenvironment (TME). Targeting the TME using colony-stimulating factor 1 receptor (CSF1R) inhibition is a promising therapy for CRPC. However, the therapeutic response to sustained CSF1R inhibition (CSF1Ri) is limited as a monotherapy. We hypothesized that one of the underlying causes for the reduced efficacy of CSF1Ri and increased oxidation in CRPC is the upregulation and uncoupling of endothelial nitric oxide synthase (NOS3). Here we show that in high-grade PCa human specimens, NOS3 abundance positively correlates with CSF1-CSF1R signaling and remains uncoupled. The uncoupling diminishes NOS3 generation of sufficient nitric oxide (NO) required for S-nitrosylation of CSF1R at specific cysteine sites (Cys 224, Cys 278, and Cys 830). Exogenous S-nitrosothiol administration (with S-nitrosoglutathione (GSNO)) induces S-nitrosylation of CSF1R and rescues the excess oxidation in tumor regions, in turn suppressing the tumor-promoting cytokines which are ineffectively suppressed by CSF1R blockade. Together these results suggest that NO administration could act as an effective combinatorial partner with CSF1R blockade against CRPC. In this context, we further show that exogenous NO treatment with GSNOR successfully augments the anti-tumor ability of CSF1Ri to effectively reduce the overall tumor burden, decreases the intratumoral percentage of anti-inflammatory macrophages, myeloid-derived progenitor cells and increases the percentage of pro-inflammatory macrophages, cytotoxic T lymphocytes, and effector T cells, respectively. Together, these findings support the concept that the NO-CSF1Ri combination has the potential to act as a therapeutic agent that restores control over TME, which in turn could improve the outcomes of PCa patients.

Cell Death and Disease (2022)13:859 ; https://doi.org/10.1038/s41419-022-05289-4

INTRODUCTION

Prostate cancer (PCa) is the most diagnosed non-skin malignancy in men [1]. Hormonal therapy is the treatment of choice for advanced PCa [2–6]. However, due to a moderate rate of success, a significant number of patients progress to castration-resistant prostate cancer (CRPC). This limited efficacy is believed to result in part from the unique ability of PCa to evolve through as-yet-unclear mechanisms in the tumor microenvironment (TME) that promotes immunologic escape. The TME is comprised of a variety of cell types of which tumor-associated macrophages (TAMs) [7] frequently make up a substantial proportion and consists of two opposing phenotypes comprising classically activated (M1-like) and alternatively activated (M2 like), which have been correlated with anti and pro- tumoral functions and with patient survival [8].

The M1/M2 dichotomy is modulated via colony-stimulating factor 1 (CSF1), which binds to the CSF1 receptor (CSF1R) to control proliferation, differentiation, and survival of macrophages [9, 10]. Previous studies support that blocking CSF1R could delay tumor growth via TAM reduction [11–15]. However, single agent CSF1R blockade showed underwhelming results in phase 2 and 3 trials. One of the reasons for the limited efficacy is the feedback mechanism induced by activated CSF1R (in tumors) that leads to recruitment of immunosuppressive and pro-tumoral TAMs and cytokines that are conducive to immune suppression [16] and are not effectively targeted by single agent CSF1R blockade. Accordingly, this suggests that modulating TAMs and cytokines that derail the efficiency of CSF1R blockade therapy could enhance therapeutic responses.

Here we assessed the impact of NO signaling pathways on the TME. Mammalian systems harbor three NOS isoenzymes that include neuronal and endothelial NOS (nNOS/NOS1 and NOS3/NOS3, respectively), which are constitutively expressed, produce nitric oxide (NO)(nM), and are regulated by Ca^{2+} binding to calmodulin [17–20]. NO has been shown to be involved in the regulation of adaptive immune responses by modulating T-cell activation, differentiation, promoting T-cell receptor-mediated signaling from the immune synapse, and M1/M2 macrophage polarization [17, 21]. The effect of NO is governed by the covalent attachment of a nitroso group to a cysteine thiol (Protein S-nitrosylation) [22, 23]. NOSs found in tumor cells, in contrast,

[1]Department of Urology, Miller School of Medicine, University of Miami, Miami, FL, USA. [2]John P Hussman Institute for Human Genomics, Miller School of Medicine, University of Miami, Miami, FL, USA. [3]The Interdisciplinary Stem Cell Institute, Miller School of Medicine, University of Miami, Miami, FL, USA. [4]Department of Medicine, Cardiology Division, Miller School of Medicine, University of Miami, Miami, FL, USA. [5]Department of Medicine, Miller School of Medicine, University of Miami, Miami, FL, USA. [6]These authors contributed equally: Fakiha Firdaus, Manish Kuchakulla, Rehana Qureshi. ✉email: Hxa287@miami.edu

Edited by Professor Anastasis Stephanou

Received: 6 July 2022 Revised: 16 September 2022 Accepted: 22 September 2022
Published online: 08 October 2022

synthesize superoxide and peroxynitrite, which results in reduced tetrahydrobiopterin: dihydrobiopterin ratio (BH4:BH2). The reduced BH4:BH2 ratio results in the uncoupling of NOSs and is observed in multiple cancer types [24]. One of the important consequences of NOS uncoupling is the reduction in NO levels and increase in oxidative stress, a situation characterized as a nitroso-redox imbalance [25, 26]. Both aid pro-tumorigenic cytokines such as NFkB [24], IFNγ [27], and TNFα [28], which further result in increased CSF1 expression in various cell types of the TME and are not effectively targeted by single agent CSF1R blockade. Together, these findings warrant to study of the impact of uncoupling of NOSs in conjunction with CSF1-CSF1R mediated M1/M2 dichotomy and TME in PCa which is unknown.

In this study, we found that NOS3 remains uncoupled in CRPC. NOS3 uncoupling results in reduced NO levels and increased oxidative stress, which eventually results in keeping the cystine residues on the CSF1R molecule in the oxidized state. This, in turn negatively influences the anti-tumor effectiveness of CSF1R blockade. Therefore, we hypothesize that concomitant blockade of the CSF1/CSF1R pathway in conjunction with an exogenous increase in NO levels may improve immune function and CRPC treatment.

MATERIALS AND METHODS

Human samples

Patients enrolled in MD-SELECT/EDRN trial were used to collecting whole blood samples. The patients were classified into different Gleason grades (6, 7, and 9) according to their PSA levels and MRI scans results. We obtained three samples corresponding to each Gleason grade. All human investigations were carried out after the IRB approval by a local Human Investigations Committee and in accord with an assurance filed with and approved by the Department of Health and Human Services. Data has been anonymized to protect the privacy of the participants. Investigators obtained informed consent from each participant. The whole blood was centrifuged at 3000 rpm to collect the white layer containing Peripheral blood mononuclear cells (PBMCs). The PBMCs were later lysed in RIPA buffer to check NOS3 and CSF1 expression using ELISA. The flash frozen prostate biopsies ($n = 5$) corresponding to Gleason grades 6 and 9 were taken from the Cancer Modeling Shared Source (CMSR) at the University of Miami. The frozen biopsies were used for doing BH4 estimation and the Griess test. The CMSR also provided the biopsy sections which were used for doing immunohistochemical staining for NOS3, CD206, CSF1, and CSF1R.

Cell culture

22R-v1 (CRL-2505), LNCaP (CRL-1740), and U937 cells (CRL-1593.2) were purchased from ATCC and maintained in RPMI 1640 medium supplemented with 10% fetal bovine serum, 100 units/ml penicillin, 100 mg/ml streptomycin and 2 mM-L glutamine. TRAMPC2 cells (CRL-2731, purchased from ATCC) were maintained in DMEM medium supplemented with 5% fetal bovine serum, 100 units/ml penicillin and100 mg/ml streptomycin.

Preparation of RNA and quantitative real-time PCR

Total RNA was extracted from cells using the TRIzol method and then reverse transcribed to complementary DNA using High-Capacity cDNA Reverse Transcription Kits (Applied Biosystems, USA) according to the manufacturer's protocol. The quantitative RT-PCR for indicated genes was performed in SYBR Universal PCR Master Mix (BIORAD, USA). Quantitation of mRNAs was performed using BIORAD™ Gene Expression Assays according to the manufacturer's protocol. Samples were analyzed using the BIORAD sequence detection system. All PCRs were performed in triplicate, and the specificity of the reaction was determined by melting curve analysis at the dissociation stage. The relative quantitative method was used for the quantitative analysis. The calibrator was the average ΔCt from the untreated cells. The endogenous control was glyceraldehyde 3-phosphate dehydrogenase (GAPDH).

Western blotting

Cells were harvested and lysed in NP-40 buffer containing phenyl methyl sulfonyl fluoride and Protease Inhibitor Cocktail (Sigma, St. Louis, MO, USA). Protein expression was studied by exposing the membranes to antibodies against AR (Abcam, ab74272), AR-V7 (GeneTex, GTX33604), pERK (Cell signaling, 4370), ERK (Cell signaling, 9102 S), pGSK-3beta (Cell signaling, 5558), p90RSK (Cell signaling, 11989), CD206 (Abcam, ab64693), VEGF (Abcam, ab46154) and GAPDH (Santa Cruz Biotechnology, SC47724). Immunoreactive bands were visualized using the Thermo Scientific Chemiluminescent Pico Kit.

Immunohistochemistry and fluorescence staining

For immunohistochemistry, tissue sections were stained with hematoxylin and eosin and analyzed by a genitourinary pathologist. For fluorescence staining, tissue slides were processed using antibodies against F4/80 (cell signaling, 70076), iNOS (abcam, 178945) and pERK (Cell signaling, 4370), followed by secondary antibodies tagged with Alexa Fluor® 488 or Alexa Fluor® 568 at room temperature for 30 minutes and 4,6-diamidino-2-phenylindole (Santa Cruz). All samples were assessed under a fluorescence microscope (Leica Microsystem, Wetzlar, Germany) at 60x magnification. Images were acquired using MetaMorph version 4.6 (Molecular Devices, Sunnyvale, CA, USA). Tumor xenograft tissues were fixed in 10% buffered formalin and embedded in paraffin. 5 µm thick sections were deparaffinized and rehydrated in sequential xylene and graded ethanol. Antigen retrieval was performed in 10 mM citrate buffer (pH 6.0) in a microwave oven. Peroxidase and non-specific protein blocking were done as per the instructions using the Abcam ABC detection kit (ab64264) and incubated with the following primary antibody dilutions: anti-Androgen Receptor (Abcam, ab74272), anti-Ki67 (Abcam, ab15580), anti-F4/80 (Cell signaling, 70076), anti-ARV7 (GeneTex, GTX33604) and anti-CD206 (Abcam, ab64693) with 1:150 dilution while a dilution of 1:50 was used for anti-Prostate-Specific Antigen (Santa-Cruz Biotech, sc7316). They were subsequently incubated with biotinylated goat anti-polyvalent secondary antibody, followed by development using DAB substrate as per the instructions on the kit. All sections were lightly counterstained with hematoxylin and mounted with Cytoseal XYL. Images were taken using a brightfield microscope (Nikon E200) at 10X and 40X magnification, and quantification was done using ImageJ software (NIH, USA).

For fluorescence staining and post-antigen retrieval, the slides were permeabilized using 0.4% triton-X with 5%BSA. After permeabilization, sections were put in a blocking solution containing 5%BSA in PBST for 30 minutes at room temperature. Afterward, incubation in primary antibodies was done overnight. The next day, slides were washed and incubated with standard fluorescent-tagged secondary antibodies for an hour at room temperature. Following washing, an antifade containing 4′,6-diamidino-2-phenylindole (DAPI) was used for mounting. Sections were imaged using a confocal microscope (Leica Microsystem, Wetzlar, Germany).

MTT assay

22RV1 and LNCAP cells were seeded in 96-wells plate in quadruplets and were treated with varying doses of GSNO or GW2580 (CSF1R inhibitor) or with a combination of GSNO and GW2580. MTT (3-(4,5-dimethylthiazole)-2,5-diphenyltetrazolium bromide) assay reagents were added, and the absorbance was measured at 562 nm after 0, 3, 5, 7, and 9 days.

Animals

The animal protocol was approved by the Institutional Animal Care and Use Committee of the University of Miami Miller School of Medicine, Miami, FL. SCID and C57BL6 (6 weeks old) mice were purchased from Jackson Laboratories (Bar Harbor, Maine). Castration experiments were performed in all the C57BL6 mice. For castration, mice were anesthetized using Isoflurane (Abbott Laboratories). The perineal region was cleaned with ethanol and a betadine scrub (VWR, AJ159778), and sterile dissecting shears were used to make a 4–5 mm incision.

Using two sterile forceps, the testes were located, and a ligature was made around the testicular vessels and the tunica albuginea that encases the testes. The testes were amputated with dissecting shears, and the scrotum was sutured closed with 6-0 Ethicon black monofilament nylon (Ethicon Inc., 1665). A local triple antibiotic was applied over the region of the wound to facilitate healing. C57BL6 mice were grouped into control and experimental groups. All the mice were grafted with 1 million TRAMPC2 cells subcutaneously. The mice were distributed randomly into the control and experimental group.The experimental group received 10 mg/kg/day of GSNO, or 40 mg/kg/day or 10 mg/kg/day GSNO + 40 mg/kg/day GW2580 treatment intraperitoneally (IP) for 2 weeks, while the control group received PBS IP. Each group had 10 mice each.

After treatment, animals survived for an additional two weeks before humanely sacrificing them. At the end time point, blood was collected via cardiac puncture, and tumor grafts, lungs, and spleen were harvested for further analysis. Tumor volume (V) was measured regularly (blinded) until the mice were sacrificed by measuring the length (L) and width (W) of the tumor with calipers by using the formula: $V = 1/2(\text{length} \times \text{width}^2)$.

Flow cytometry analysis for immune markers

For making single cell suspension from TRAMPC2 tumors, a piece of tumor was taken and minced with scissors or a blade. These minced tumors were digested using a digestion buffer containing collagenase by agitation at 37 °C for 1.5 h and vortexing for a min, every 30 min. It was followed by adding RBC lysis buffer and 0.25%trypsin-EDTA and incubating again @ 37 °C for 15 mins. Lastly, 5 ml of chilled FACS buffer (PBS + 2% FBS) was added, and the digestion mixture was then filtered with a 40 µm cell strainer. The cells were allowed to spin down at 450 g for 5 min, and the collected pellet was resuspended in 2 ml FACS buffer. These isolated single cells were incubated with different antibodies following standard staining protocols for intra-cellular and membrane-bound antibodies. The details of the antibodies are mentioned in Supplementary Table 2. Following staining, the cells were fixed in a standard fixing solution containing 4% paraformaldehyde and taken for flow cytometry. The analysis was done using a CYTEK Aurora flow cytometer.

Griess test

20 µL of Griess Reagent (Thermo Fischer Scientific G-7921) and 150 µL of the nitrite-containing sample were mixed in a microplate (sample capacity at least 300 µL per well). The mixture was incubated for 30 minutes at room temperature in the dark. To prepare a photometric reference sample, 20 µL of Griess Reagent was mixed with 280 µL deionized water. The absorbance of the nitrite-containing samples relative to the reference sample was measured in a spectrophotometric microplate reader at 548 nm. To convert absorbance readings to nitrite concentrations, the method recommended by the manufacturer was used.

Tetrahydrobiopterin (BH4) ELISA

The kit (Catalog No. ABIN6957559, Antibodies online) is a competitive inhibition enzyme immunoassay technique for the in vitro quantitative measurement of tetrahydrobiopterin in serum, plasma, tissue homogenates, cell lysates, cell culture supernatants. The amount of lysates used was 100ug of protein.

Human NOS3/NOS3 ELISA

Peripheral blood mononuclear cells (PBMCs) collected from patient blood samples were used for the estimation of NOS3 levels (Catalog # EH169RB, Thermo Fischer Scientific, USA). The steps followed were according to the kit instructions. 100 µg of cell lysate was used for quantification.

M-CSF (CSF-1) Human ELISA

Peripheral blood mononuclear cells (PBMCs) collected from patient blood samples were used for the estimation of CSF-1 levels (Catalog # EHCSF1, Thermo Fischer Scientific, USA). 100 µg of cell lysate was used for the assay. The steps followed are the same as mentioned in the instruction manual.

Cytokine antibody array

Proteins were isolated from tumors of the CRPC mice that had received treatment with PBS and GSNO. After quantification using Bradford assay, 2.5 mg/ml protein lysates were screened for secreted protein using RayBio Human Cytokine Array C5, Code: AAH-CYT-5-2 (RayBiotech, Norcross, GA, USA) according to the manufacturer's instructions. The blots were analyzed using ImageJ software (National Institutes of Health, Bethesda, MD, USA). A total of 80 molecules were selected for detection namely: ENA-78, G-CSF, GM-CSF, GRO, GRO-alpha, I-309, IL-1alpha, IL-1beta, IL-2, IL-3, IL-4, IL-5, IL-6, IL-7, IL-8,IL-10, IL12-p40, IL-13, IL-15, IFN-gamma, MCP-1, MCP-2, MCP-3, M-CSF, MDC, MIG, MIP-1 beta, MIP-1-delta, RANTES, SCF, SDF-1, TARC, TGF-beta 1, TNF-alpha, TNF-beta, EGF, IGF-1, Angiogenin, Oncostatin M, TPO, VEGF, PDGF-BB, Leptin, BDNF, BLC, CK beta 8-1, Eotaxin, Eotaxin-2, Eotaxin-3, FGF-4, FGF-6, FGF-7, FGF-9, Flt-3 Ligand, Fractalkine, GCP-2, GDNF, HGF, IGFBP-1, IGFBP-2, IGFBP-3, IGFBP-4, IL-16, IP-10, LIF, LIGHT, MCP-4, MIF, MIP-3-alpha, NAP-2, NT-3, NT-4, Osteopontin, Osteoprotegerin, PARC, PIGF, TGF-b 2, TGF- b 3, TIMP-1, and TIMP-2 respectively.

Biotin switch assay and SNO protein purification

The S-nitrosylated proteins were visualized by biotin-switch assay following the manufacturer's guidelines (S-Nitrosylated Protein Detection Kit (Biotin Switch), Item No. 10006518, Cayman Chemical, Ann Arbor, MI, USA) [29, 30]. A small piece of tumor tissue or cell pellet was taken and washed twice with Wash Buffer. The pellets were resuspended in "Buffer A containing Blocking Reagent" and incubated for 30 min at 4 °C with shaking. The incubated samples were centrifuged at 130,000×rpm for 10 min at 4 °C, and the supernatant was transferred to 15 ml centrifuge tubes. Two milliliters of ice-cold acetone were added to each sample, and the mixture was incubated at −20 °C for at least 1 h. The protein of each sample was pelleted by centrifugation for 10 min at 4 °C. "Buffer B containing Reducing and Labeling Reagents" was added to resuspend the proteins, with incubation for 1 h at room temperature. The biotinylated protein was precipitated by acetone and rehydrated with the appropriate amount of Wash Buffer.

A total of 40 µg of protein was used for labeling and running the standard western blot for detecting the nitrosylated protein.

RNA sequencing and enrichment analysis

Fastq files were downloaded from Illumina's BaseSpace cloud application. FastQC was performed on the fastq files to ensure acceptable base quality and GC content and to check for adapters. Adapters were trimmed using the Trim_Galore software to remove the Illumina Universal Adapter. After adapter trimming, Fastq_screen was performed to check for bacterial contamination. Once no contamination was confirmed, general alignment was performed using the STAR RNAseq aligner to the hg19 genome. During this alignment, raw counts were produced against the GENCODE gene features (v19) and reformatted into a matrix for further statistical processing. After alignment, PicardTools was used to calculate sample-by-sample alignment quality metrics statistics. Differential expression was performed on the raw count matrix using the edgeR software. Statistical significance was defined as any gene feature that had an FDR value of below 0.05. Gene set enrichment analysis was performed by means of Broad's GSEA executable jar file using MSigDB as the reference database. Normalized log2CPM values were used as the expression values. These CPM values were filtered by log2CPM of 1 to limit the noise of the data used for enrichment. Three sets of runs were completed against hallmark genes (h).

Activation of monocytes for M1/M2 polarization

U937 cells were activated using different cytokines as done by previous studies. The cells were treated in RPMI 1640 medium supplemented with 5% cFBS, in 100 mm flat-bottom culture plates. Activation treatments consisted of (1) no stimulation control (mock); (2) PMA 20 ng/mL for 48 h (PMA-only control); (3) pre-treatment with PMA 20 ng/mL for 48 h, followed by LPS 50 ng/mL and IFN-γ10 ng/mL for 48 h (condition favoring M1 polarization, M1 cocktail); (4) pre-treatment with PMA 20 ng/mL for 48 h, followed by IL-4 25 ng/mL and IL-13 25 ng/mL for 48 h (condition favoring M2 polarization, M2 cocktail). In addition to these treatments, three-drug combinations, i.e., GSNO (50 µM), CSF1Ri (0.5 µM), and a combination of both GSNO and CSF1Ri were also used to check their effect on monocyte activation as well as macrophage polarization.

Macrophage polarization study for studying the interaction of androgen receptor (AR) and S-nitrosoglutathione (GSNO)

For this study, U937 cells (purchased from ATCC) were used as a model for monocyte-macrophage differentiation. The study was divided into two steps: a) Collection of conditioned media and cell lysates from 22Rv1 cells and b) Treatment of U937 cells with conditioned media from 22Rv1. For preparing the 22Rv1 cell conditioned media (CM), 3.0 × 105 cells were seeded into 6-well culture plates and allowed to adhere overnight. The next day, the cells were starved using charcoal-stripped FBS for about 12 hours and then 2 ml of medium containing 1% FBS. The cells were treated with 4 µM enzalutamide (ENZA, Selleckchem, MDV3100) in the presence or absence of 50 µM GSNO. The untreated 22Rv1 cells served as control. The media was collected 48 h later. The supernatant was centrifuged at 1800 rpm for 10 min and was collected as CM. U937 cells were treated with the collected CM from these different treatment conditions. The cells were collected at 48 h for analysis of M2 macrophage marker, CD206 (Abcam, ab64693) and AR (Abcam, ab74272).

Organoid cultures using 22Rv1 cells for Immunohistochemical (IHC) staining

The organoid cultures using 22Rv1 cells were generated using the protocol followed by Ma et al. (2017). A total of 250,000 cells/ml were suspended in thawed Matrigel, and a drop was added to each well of a 24-well plate. Organoids were maintained in adDMEM/F12 media with growth factors and 10 µM Y-27632 dihydrochloride. The media was refreshed every 2-3 days. 7 days after initial plating, an organoid culture medium without Y-27632 dihydrochloride was used. The culture ended on day 14. Later the organoids were fixed in 4% paraformaldehyde and processed for paraffin embedding and sectioning.

Site-directed mutagenesis

CSF1R ORF clone (OHu24034, NM_001349736.1) was procured from GenScript Biotech (NJ, USA). Site-directed mutagenic changes were performed to incorporate 3 cysteine deletions at C224, C278, and C830 (as determined by GPS-SNO 1.0 software with a high threshold) using Quick Change Lightning Multi Site-Directed Mutagenesis Kit (Agilent Technologies, USA), as previously described [31]. Briefly, 40 ng plasmid was subjected to PCR amplification as per standard kit guidelines using mutagenic primers 5′-tgcccagatcgtgtcagccagcagcg-3′, 5′-cgctgctggctgacacgatctgggca-3′; 5′-cgttgctggccacggagtagttgccg-3′, 5′-cggcaactactccgtggccagcaacg-3′ and 5′-ctctgaaccgtgtagacgtcaaagatgctctctg-3′, 5′-cagagagcatctttgacgtctacacggttc agag-3′ for cysteine del1, del2 and del3 respectively. Following PCR, 10 µl of the product was subject to DpnI digestion for 5 min at 37 °C and transformed into chemically competent DH5α cells (NEB, USA) by heat shock at 42 °C for 30 sec. The resulting transformants were grown in SOC media for 1 hr at 37 °C and selected overnight on LB agar plates containing 100 µg/ml of Ampicillin. The following day, single colonies were selected and further grown in LB broth containing 100 µg/ml of Ampicillin for 12 hours. Plasmid isolation and purification were done using a plasmid miniprep kit (Qiagen, Germany) as per standard instructions. Sanger sequencing for confirmation of deletion was done by Genewiz, USA. For verification of these deletions, the confirmed wild-type, as well as mutant clones, were transfected in 22Rv1 cells using Lipofectamine 3000 reagent. After transfection, cells were treated with/without 50 µM GSNO, and cells were collected after 48 h to do western blots using anti-Androgen Receptor (Abcam, ab74272) anti-beta Actin antibody (Cell Signaling Technology, 4970) antibodies.

Statistical analysis and calculation of sample size

GraphPad Prism (GraphPad Software) was used for statistical analysis. All data are presented as means ± SEM. The statistical significance between the two groups was determined by an unpaired two-tailed *t-test*. Multiple group comparisons were performed using a one-way analysis of variance with Tukey's least significant difference test. For the GSNOR activity assay, the area under the curve (AUC) was calculated by taking $Y = 1$ as the baseline, followed by a non-linear regression 1 phase decay. In all cases, the variance similar between the groups that are being statistically was compared. In all cases, $p < 0.05$ was considered statistically significant.

RESULTS

Prostate cancer progression is associated with increased CSF1 concentration and Nitric oxide synthases

The expression of CSF1 and all 3 NOS isoforms (NOS3, NOS2, and NOS1) were evaluated using RNA sequencing data for Prostate adenocarcinoma from The Cancer Genome Atlas (TCGA). With increasing cancer grade (Gleason 6-10), the expression of CSF1 and NOS3 increased (Fig. 1A, Supplementary Fig. 1). The CSF1, under physiological conditions, plays a role in cell survival, proliferation, differentiation, and functions of the mononuclear cells, and therefore its higher expression in patients without cancer is not surprising [32–34]. Additionally, peripheral blood mononuclear cells (PBMCs) isolated from the blood of healthy individuals and patients with primary (Gleason 6), mid (Gleeson 7), or distant metastasis (Gleason 9) PCa ($n = 2$ per condition) showed that both CSF1 and NOS3 were significantly increased ($p < 0.05$) in high-grade PCa patients (Fig. 1B–D) compared to patients with low-grade PCa. We also evaluated the expression of NOS3 in patient biopsies from Gleason 6 and Gleason 9 ($n = 3$); and found an overall increase in its expression (***$p \leq 0.001$) (Fig. 1E). These findings indicate that CSF1 and NOS3 production is elevated in proportion to prostate cancer disease progression.

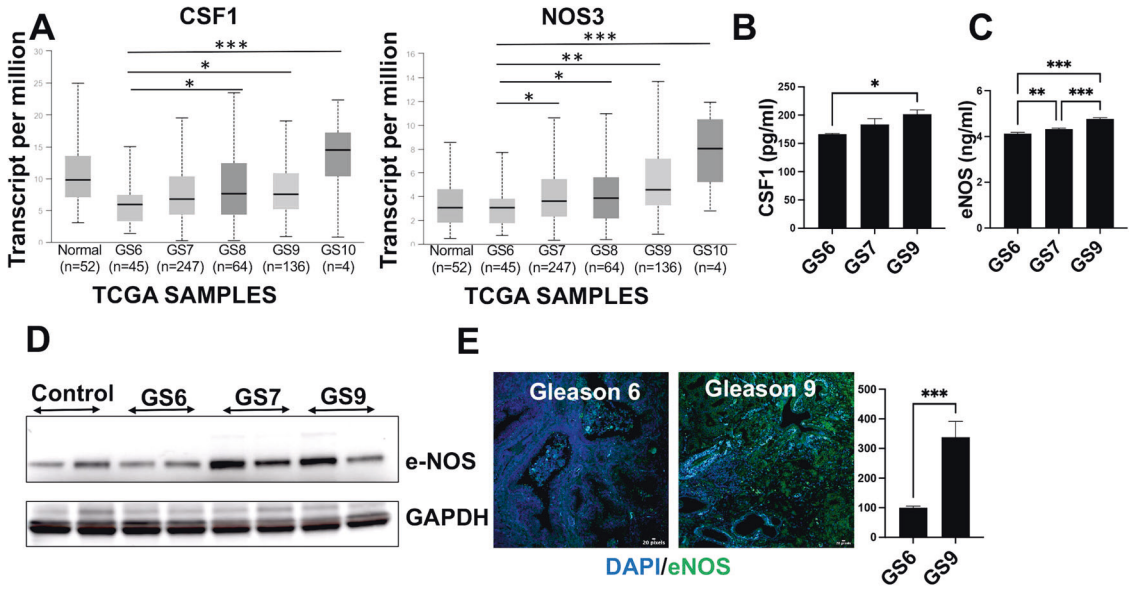

Fig. 1 Prostate cancer progression is associated with increased CSF1 concentration and Nitric oxide synthases. The relative expression of CSF1 and NOS3 was studied using RNA sequencing data for Prostate adenocarcinoma from The Cancer Genome Atlas (TCGA). **A** Graphs showing expression of CSF1 and NOS3 across different Gleason Grades. **B** Quantification of CSF1 and **C** NOS3 was done by enzyme-linked immunosorbent assay (ELISA) performed in PBMCs collected from different patient blood samples with different Gleason grades ($n = 2$). CSF1 levels are expressed as pg/ml, while NOS3 levels are expressed as ng/ml. **D** Western blot following immuno-precipitation of Peripheral Blood Mononuclear Cells (PBMCs) showing the expression of NOS3 (NOS3) ($n = 2$). **E** Immunofluorescent staining images showing expression of NOS3 (green) in patient biopsies from Gleason Grade 6 and 9. Data are means ± SEM. *n*, number of samples. GS, Gleason grade. *$p < 0.05$; **$p < 0.01$; ***$p < 0.001$.

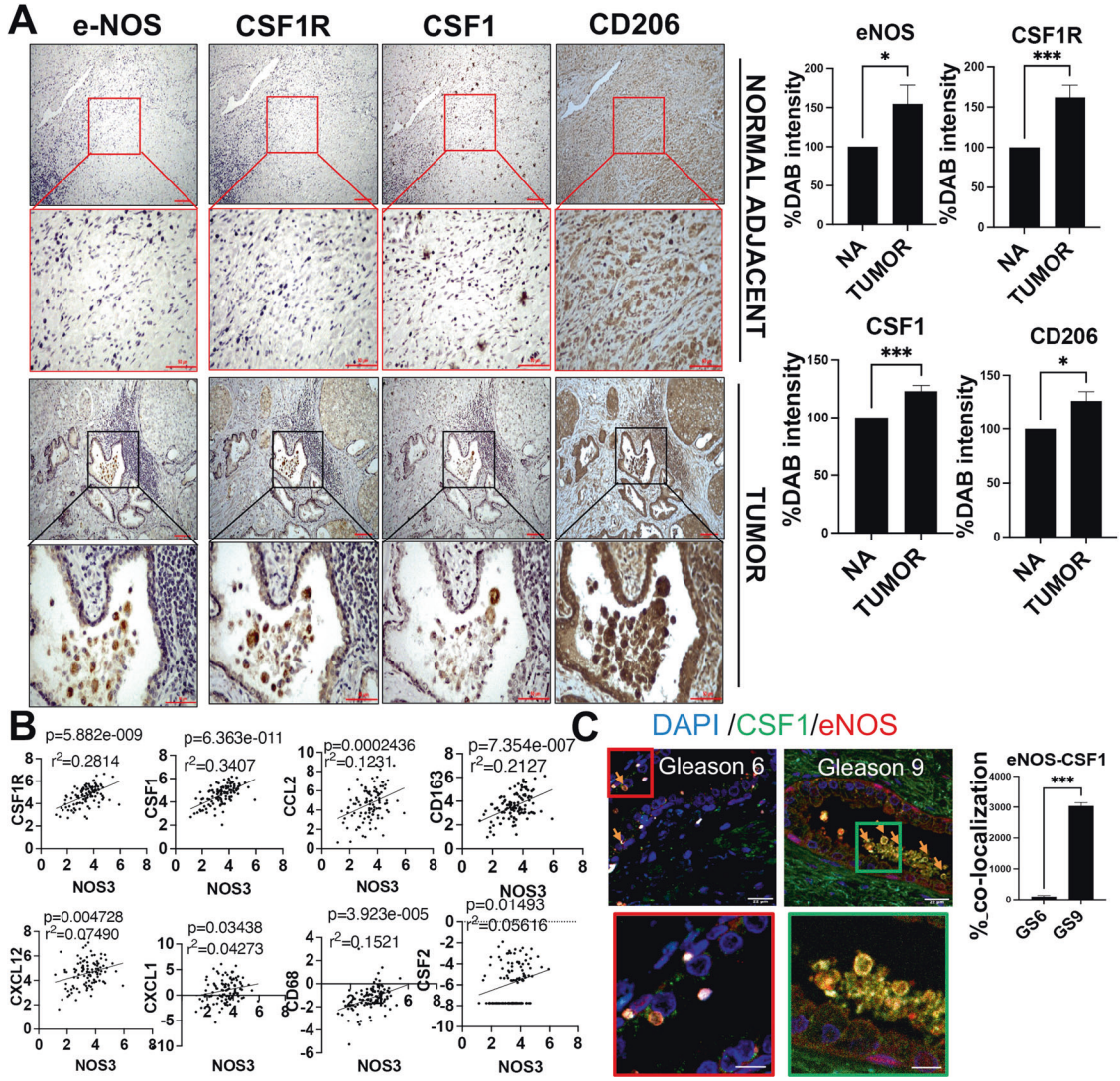

Fig. 2 NOS3 expression in prostate cancer biopsies is correlated with enrichment of CSF1$^+$, CSF1R$^+$, and CD206$^+$ cells. A Representative images of NOS3, CSF1R, CSF1, and CD206 immunostaining selected from a tumor region with either high or low NOS3 expression in a patient biopsy sample. The red and blue square in the upper panel indicates a region of interest that has been magnified in the lower panels. Scale bar, 100 µm. **B** Matrix of scatterplots showing correlations between CD8A, CD8B, CSF1, CSF1R, CD68, and CD163 gene expression specific to high-grade prostate cancer (Gleason grade 9) of TCGA. The correlation was assessed using Spearman's correlation coefficient. Black lines indicate the local regression (LOESS) fit. *P*, *P* value; *n*, number of samples; r^2, Spearman's correlation coefficient. **C** Representative multiplexed fluorescence staining images of tumor tissue from one prostate biopsy patient stained with 4′,6-diamidino-2-phenylindole (DAPI) (blue), and antibodies against CSF1 (green) or NOS3 (red). Percentage of co-localization for CSF1 + NOS3 + cells are represented for the patients listed in Table S1 ($n = 3$). Data are means ± SEM of three images per tumor area for each patient. *$p < 0.05$; ***$p < 0.001$.

The high number of NOS3$^+$ cells in high-grade PCa is correlated with the enrichment of CSF1$^+$ and CSF1R$^+$ cells

Increased expression of CSF1 and CSF1R were found to be specific to cancer regions in high-grade PCa (e.g., Gleason 9) in comparison to normal adjacent regions ($n = 3$ patients) (Supplementary Fig. 2A). Additionally, with an increasing grade of PCa (Gleason 6, 7, and 9), the expression of inflammatory (M2) macrophages (CD206) increases (Supplementary Fig. 2B). To determine whether the expression of NOS3 is correlated with CSF1, CSF1R, and CD206, chromogenic immunohistochemistry (IHC) was performed using specimens from normal adjacent and metastatic regions of high-grade PCa ($n = 3$). In this analysis, high-grade cancer regions with higher expression of NOS3 had elevated CSF1, CSF1R, and CD206 (Fig. 2A). Furthermore, RNA sequencing analysis from TCGA data showed that the expression of NOS3/NOS3 positively correlated with the expression of CSF1, CSF1R, CD163, and several other tumor-promoting immune cell markers in high-grade PCa (Gleason 9) (Fig. 2B). Moreover, immunofluorescence staining (IF) demonstrated that a positive correlation between NOS3 and CSF1 is specific to high-grade PCa ($n = 3$ specimen for Gleason grades 6 and 9) (Fig. 2C). This correlation was also observed in tumor grafts from hormone (androgen)-insensitive cells (neuroendocrine PCa (H660 cells) grafted in castrated SCID mice) (Supplementary Fig. 2C, D). These results strongly support that the abundance of NOS3 positively correlates with TAM in human PCa.

Tumor cells are a source of NOS3 in human prostate cancer

Next, in order to evaluate whether PCa cells could be a source of NOS3, we performed IF on histological sections of three Gleason 9 specimens. PCa cells were identified by their expression of the FOXM1 [35]. We found that out of 73.77% FOXM1 + PCa cells, 54.28% expressed NOS3 in all three patient biopsy sections (Fig. 3A). We then assessed CSF1 in relation to FOXM1 cell

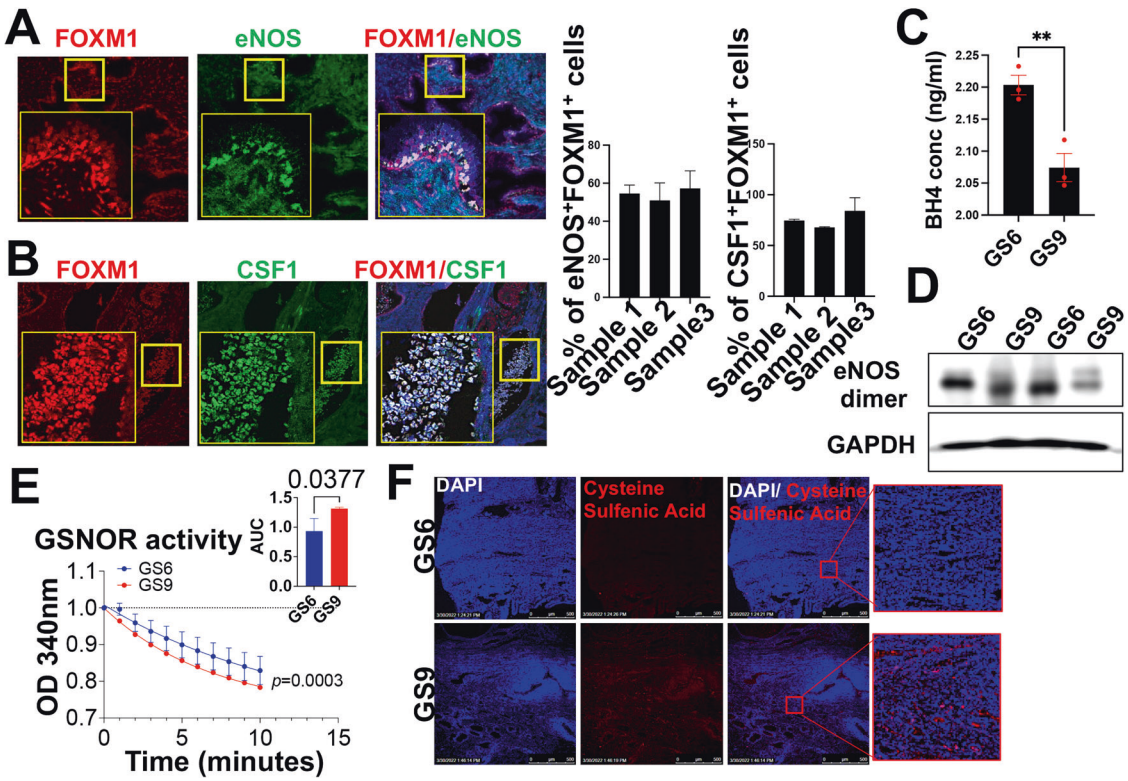

Fig. 3 Tumor cells are a source of NOS3 in human prostate cancer. A, **B** Representative multiplexed fluorescence staining images of tumor tissue from one prostate biopsy patient stained with 4′,6-diamidino-2-phenylindole (DAPI) (blue) and antibodies against FOXM1 (red) and NOS3/CSF1 (green). Percentage of FOXM1 + prostate cancer cells that are also NOS3 + as well as CSF1 + in prostate adenocarcinomas ($n = 3$) from the patients listed in Table S1. Data are means ± SEM of three images per tumor area for each patient. Scale bar, 22 μm. **C** BH4 concentration was estimated using a competitive enzyme-linked immunosorbent assay (ELISA) using prostate biopsy lysates ($n = 3$). $^{**}p < 0.01$. Scale bar, 22 μm. **D** Uncoupling of NOS3 as shown by dimers using prostate biopsies from different Gleason grades. The lysates were run at low temperatures without beta-mercaptoethanol to look for dimers. **E** GSNOR activity was measured and recorded at 340 nm for 10 minutes in prostate biopsies from Gleason grade 6 and Gleason grade 9 ($n = 3$). **F** Representative immunofluorescent images for patient biopsies (Gleason grade 6 and 9) stained with 4′,6-diamidino-2-phenylindole (DAPI) (blue), and Cysteine sulfinic acid (red). Scale bar 100 μm.

abundance and found that the CSF1 expression was higher in regions with higher FOXM1 expression (Fig. 3B).

NOS3 in human prostate cancer is in an uncoupled state

The primary function of NOSs is the synthesis of nitric oxide (NO), which requires NOS dimerization. A reduced ratio of BH4:BH2 in several cancer types can destabilize the NOS subunits leading to uncoupling, which in turn switches the enzymatic activity toward superoxide ($O2^{-}$) generating enzyme [24, 36]. To evaluate the degree of uncoupling of NOS3 in high-grade human PCa, we quantified the level. This assessment showed a significant reduction of BH4 in patients with distant metastasis compared to specimens from primary PCa (Gleason 6) ($n = 3$ each)(Fig. 3C). This was further reflected by the reduced dimerization of NOS3 in distant metastasis specimens compared to primary PCa (Fig. 3D). Next, we tested the activity of the S-nitrosoglutathione reductase in proteins from primary and metastatic human PCa tissues ($n = 3$ each), and showed an enhanced GSNOR activity in metastatic specimens, suggesting a higher depletion rate of GSNO (Fig. 3E). Therefore, reflecting that in high-grade human PCa, NOS3 becomes upregulated but uncoupled with the increased GSNOR activity, suggesting a profound depletion in intracellular NO availability or nitroso-redox imbalance.

Uncoupled NOS3 could negatively influence the anti-tumor effectiveness of CSF1R blockade therapy against CRPC

In the NOS3 enzyme, NADPH-derived electrons flow from the reductase domain toward the oxygenase domain, and in the presence of BH4, these electrons react with oxygen and L-arginine and lead to the formation of L-citrulline and NO [37]. However, in the absence or reduced levels of BH4 (as observed in high-grade PCa), oxygen undergoes oxidation and yields superoxide [38, 39]. In this context, considering a strong and positive correlation between NOS3 and the CSF1-CSF1R axis and based on findings that suggest that neo-adjuvant CSF1R inhibition is minimally effective against high-grade PCa [40], we hypothesize that increased oxidation because of uncoupling of NOS3 could reduce the efficiency of CSF1R blockade. To study this, first we evaluated the extent of oxidation in histological sections from primary or metastatic PCa specimens ($n = 3$ each) through IF with antibody against Cysteine Sulfenic Acid (CSA) [41, 42]. This analysis showed an increase in oxidation pockets in high-grade PCa (Fig. 3F). Importantly, CSF1R expression was found to be localized in these oxidized pockets. Furthermore, we generated prostate organoids using 22RV1 (CRPC) cells. These organoids were exposed to single agent CSF1R blockade (GW2580). Immunostaining on organoid sections showed minimal changes in the expression of CSA or NOS3 upon CSF1R blockade (Fig. 4A). Next, we tested the effects of CSF1R blockade in CRPC in-vivo models (castrated C57BL6 mice were grafted with TRAMPC2 cells) (Fig. 4B). Exposure to CSF1Ri (40 mg/kg/day IP) was able to reduce the tumor burden (Fig. 4C), but GSNOR activity remained unchanged (Fig. 4D). Furthermore, like organoids, IHC on murine tumor grafts demonstrated no change in oxidation pockets in the control or treatment group (Fig. 4E). Together the results suggested that NOS3 is upstream to the CSF1-CSF1R axis and CSF1R blockade has minimal influence on oxidation. Furthermore, despite the reduction in tumor burden upon CSF1R blockade, there was a

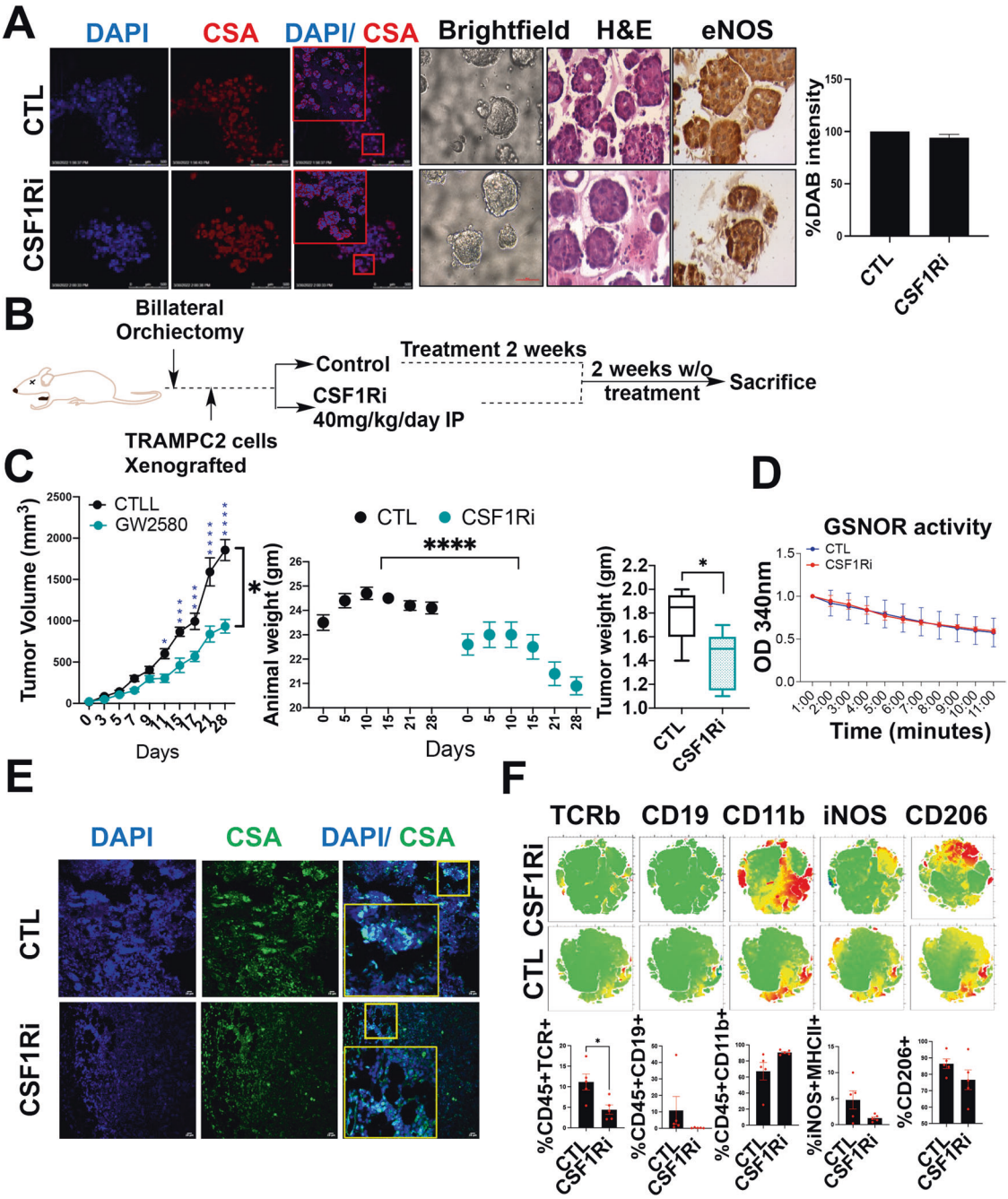

Fig. 4 CSF1R inhibition reduces PCa tumor burden but potentiates pro-tumorigenic signatures. A Representative bright-field, H and E and immunofluorescent images for 22Rv1 derived organoids stained with 4′,6-diamidino-2-phenylindole (DAPI) (blue) and Cysteine sulfinic acid (red) showing oxidation status. The chromogenic substrate DAB (brown) represents the expression of NOS3 in untreated control and CSF1Ri treated organoids. Scale bar 400 μm. **B** Experimental plan. **C** Mean change of tumor volume (±SEM; versus tumor volume at treatment start) in C5BL6 mice treated as indicated. Vehicle ($n = 5$), α-CSF1R ($n = 5$). Animal weight changes throughout the experiment from Day 1 to Day 28. Tumor weight plotted as Mean ± SEM ($n = 5$) measured at the end of the experiment. **D** GSNOR activity was measured at 340 nm for 10 minutes using tumor lysates treated with vehicle and CSF1R inhibitor ($n = 3$). **E** Representative immunofluorescent images for tumor sections for mice treated with vehicle and CSF1R inhibitor and stained with 4′,6-diamidino-2-phenylindole (DAPI) (blue) and Cysteine sulfinic acid (red) ($n = 3$). **F** Representative tSNE plots and graphs for various immune cell surface markers (TCRβ, CD19, CD11b, iNOS, and CD206) for tumor cells isolated from mice tumors treated with vehicle and CSF1R inhibitor.

minimal change in the expression of AR, pERK, p-GSK, VEGF, ARV7, and Ki67 (Supplementary Fig. 3A, B). Moreover, the cytokine array showed a minimal impact of CSF1R blockade on several tumor-promoting cytokines such as ENA-78, BLC, IP-10, Oncostatin M, FGF-6, IGFBP-3, RANTES, Osteopontin, GCP-2, IL-15, MCP-4, NT-4, TGF- b 3, IL-3, SCF, IL12-p40, IGFBP-4, FGF-4, SDF-1, PDGF-BB, IL-1beta, PARC, TPO, IFN-gamma, FGF-7, and IL-2 respectively (Supplementary Fig. 3C). The role of each of these cytokines is summarized in Supplementary Table 1.

Next, tumor grafts from control and treatment groups were subjected to comprehensive immunophenotyping, which utilizes a standardized panel of antibodies against each of the immune cell types (Supplementary Table 2). Results demonstrated minimal effects (no significant change) of CSF1R blockade on several of the

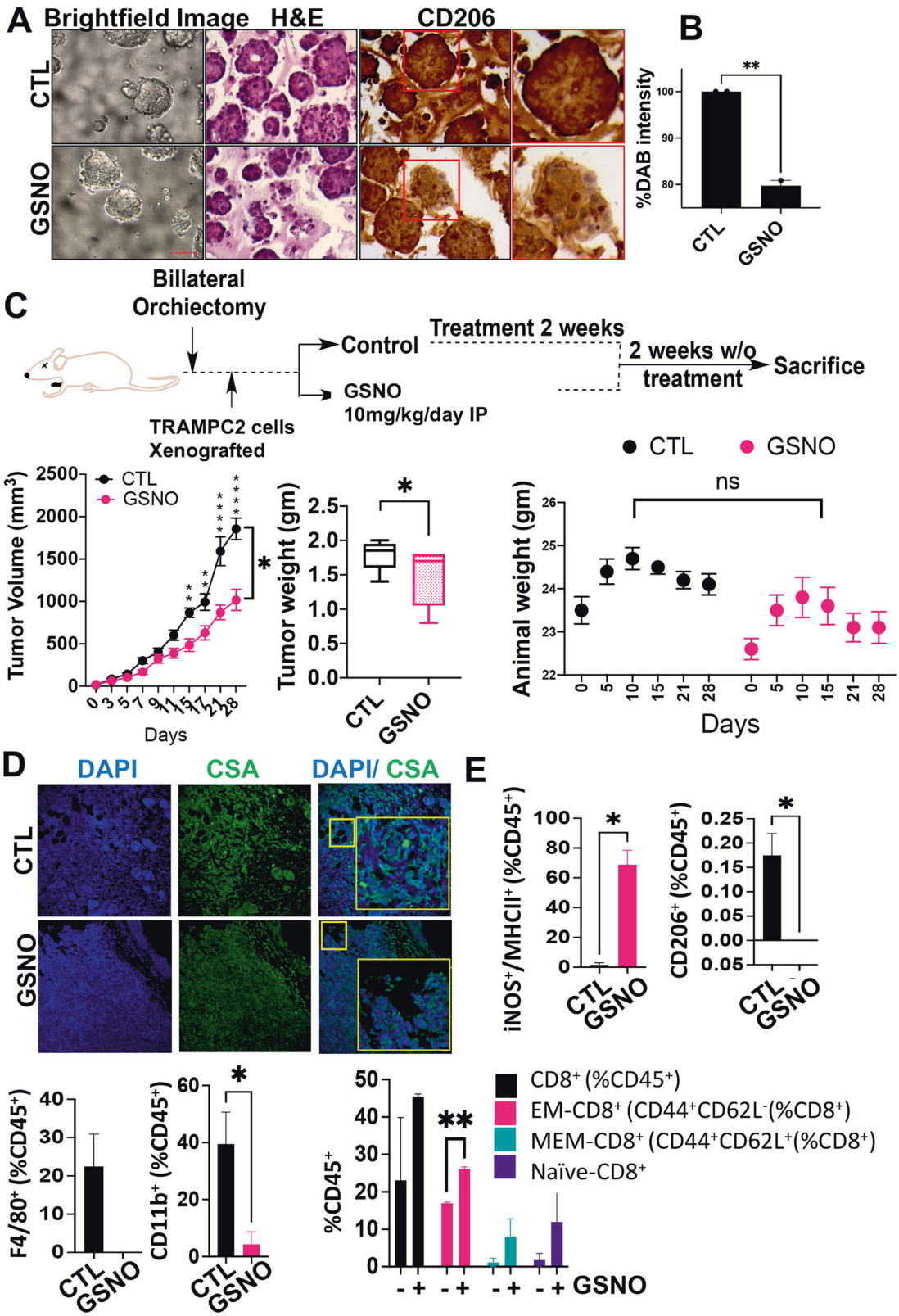

cell types ($CD206^+$ (%$CD45^+$)(M2 macrophages), $iNOS^+$/MHC-II^+ cells (%$CD45^+$)(M1 macrophages), $CD11b^+$(%$CD45^+$)(myeloid cells), % B cells and % T cells) (Fig. 4F, Supplementary Fig. 3D). Together the results suggested that the low efficiency of CSF1R blockade could potentially be accounted for increased oxidation and reduced NO levels, which results from NOS3 being in an uncoupled state.

Exogenous induction of NO overcomes the negative effects of NOS3 uncoupling and demonstrates tumor inhibitory role against CRPC

We next determined if exogenous administration of a low molecular weight S-nitrosothiol could rescue the negative effects of increased oxidation and NOS3 uncoupling on the CSF-CSF1R

Fig. 5 Increased NO reduces PCa tumor burden and pro-tumorigenic signatures. A Representative bright-field, H and E and immunofluorescent images and DAB chromogenic substrate showing expression of CD206 in 22Rv1 derived organoids. Scale bar 400 μm. **B** Graph showing %DAB intensity for CD206 expression. Data are ±SEM. Scale bar 400 μm. **C** Mean change of tumor volume (±SEM; versus tumor volume at treatment start) in C5BL6 mice treated as indicated in the flow diagram. Vehicle ($n = 5$), S-nitrosoglutathione, GSNO ($n = 5$). Animal weight plots throughout the experiment from Day 1 to Day 28. Tumor weight plotted as Mean ± SEM ($n = 5$) measured at the end of the experiment. **D** Representative immunofluorescent images for tumor sections for mice treated with vehicle and GSNO and stained with 4′,6-diamidino-2-phenylindole (DAPI) (blue) and Cysteine sulfinic acid (red) ($n = 3$). **E** Graphs showing the percentage of various immune cell populations in tumor grafts representing percentage of iNOS + /MHCII + (M1-macrophages), CD206+, F4/80+ (M2-macrophages) and CD11b + myeloid cells. Also, the cytotoxic T cell population (CD8+), EM-CD8+ (CD44+ CD62L−), MEM− CD8+ (CD44+ CD62L+), and naive CD8+ are represented in GSNO tumors treated as indicated and analyzed by flow cytometry (Mean ± SEM). Statistical analysis by Student's *t*-test. ***$P < 0.001$; **$P < 0.01$; *$P < 0.05$. ns = not significant.

axis. For this, we focused on CSF-CSF1R induced functions which primarily include macrophage polarization, to promote angiogenesis, tissue remodeling, and immune suppression [43]. In this context, prostate organoids (from 22RV1 cells) were exposed to an exogenous source of NO (S-nitrosoglutathione (GSNO)). In these experiments, we observed a significant reduction (**$p \leq 0.01$) in CD206 expression upon treatment (Fig. 5A, B). Second, we used U937 cells (model for monocyte-macrophage differentiation) and treated them with Phorbol-12-Myristate-13-Acetate (PMA) in the presence of M1 or M2 macrophage-inducing cocktails (Supplementary Fig. 4A). These cells were then exposed to GSNO (50 μM), and the percentage shift in the population of M1 ($CD68^+$) or M2 ($CD206^+CD163^+$) cells was evaluated. This experiment revealed a significant increase in M1 and a reduction in M2 macrophage populations (Supplementary Fig. 4A), suggesting that an exogenous increase in NO could inhibit macrophage polarization in-vitro. Furthermore, studies suggest that AR signaling in macrophages promotes PCa cell migration and invasion [44–46]. To study if the exogenous increase in NO could inhibit AR signaling in macrophages to influence macrophage polarization, we exposed U937 cells to conditioned media (CM) from 22RV1 cells which were treated with enzalutamide (AR antagonist) or with GSNO (Supplementary Fig. 4B). Both enzalutamide and GSNO treatment reduced the expression of AR and CD206 in 22RV1 and U937 cells (Supplementary Fig. 4C). Third, we asked if exogenous induction of NO could inhibit tumor growth. For this, we tested the effects of GSNO on murine CRPC in-vivo models. Results showed that GSNO inhibited tumor burden by showing a significant decrease (*$p \leq 0.05$) in the tumor volume and tumor weight (Fig. 5C). The tumor grafts from the GSNO treatment group showed reduced oxidation pockets compared to the control group (Fig. 5D). Moreover, the expression of AR, ARV7, and Ki67 was reduced upon GSNO treatment (Supplementary Fig. 5A). Next, we subjected the tumor grafts to immunophenotyping. Results showed that GSNO increased the percentage of $iNOS^+/MHC\text{-}II^+$ cells ($\%CD45^+$) (M1 macrophages), tumor-infiltrating lymphocytes ($CD8^+(\%CD45^+)$ cells), EM-$CD8^+$ ($CD44^+CD62L^-$), MEM-$CD8^+$ ($CD44^+$ $CD62L^+$), and naive $CD8^+$ cells ($\%CD45^+$) and reduced the percentage of $CD206^+$ ($\%CD45^+$)(M2 macrophages), $F480^+$ ($\%CD45^+$)(macrophages), and $CD11b^+(\%CD45^+)$(myeloid) cells (Fig. 5E). Together the results suggested that an exogenous increase in NO could rescue increased oxidation; inhibit macrophage polarization; and have tumor inhibitory effects against CRPC.

Nitric oxide S-nitrosylates CSF1R to induce tumor inhibitory functions

One of the key mechanisms of action of GSNO is through the coupling of a nitroso moiety from NO-derived metabolites to a reactive cysteine leading to the formation of an S-nitrosothiol (SNO), a process commonly known as S-nitrosylation [29, 47]. Considering a strong correlation between un-coupled NOS3 and CSF1-CSF1R signaling and the inhibitory impact of both GSNO and CSF1R blockade against M1-M2 dichotomy, we hypothesized that GSNO could potentially S-nitrosylate CSF1R to inhibit CRPC tumor burden, overall oxidation, and macrophage dichotomy. For this, the biotin-switch assay was performed to measure S-Nitrosylated (S-NO) CSF1R proteins from tumor grafts from mice exposed to GSNO treatment. Results confirmed that GSNO treatment induced S-nitrosylation of the heavy chain of CSF1R (Fig. 6A). Next, we screened CSF1R to identify potential cystine sites using GPS-SNO 1.0 software which conformed to an acid-base nitrosylation conservative motif (14, 29). A total of 20 cystine sites were identified on the CSF1R structure, with three sites Cys224, Cys278, and Cys830, having a high predicted threshold (cutoff 2.443) for being S-nitrosylated (Fig. 6B and Supplementary Table 3). Cysteine mutations were generated for Cys224, Cys278, and Cys830 by site-directed mutagenesis. A topology map of CSF1R indicated that the location of the 3 mutated cysteines in the CSF1R structure is shown in Fig. 6C. Next, we characterized the cellular localization of these mutants (Cys224, Cys278, and Cys830) in 22RV1 cells to determine whether cysteine mutations lead to a disruption of protein 3D structure. All the mutants localized primarily to the nucleus of the cells in a pattern like that of wild-type CSF1R protein (Fig. 6D). Further, we transfected the 22RV1 cells with the CSF1R plasmids (wild type and three mutants), followed by exposing the cells to vehicle or GSNO for 48 hours. Biotin-switch assay confirmed that reduced GSNOR activity was directly correlated with blocked Cys224, Cys278, and Cys830 sites which further inhibited the GSNO-induced S-nitrosylation of CSF1R (Fig. 6E).

Next, to confirm if S-nitrosylation of CSF1R at Cys224, Cys278, and Cys830 is relevant for the effective reduction of tumor-promoting cytokines, we transfected 22RV1 cells with CSF1R plasmids (wild-type and three mutants) and exposed the cells to vehicle or CSF1R blockade (GW2580, 0.5 μM) for 48 hours. Post-treatment, protein lysates were subjected to a cytokine antibody array. Results (Fig. 6F) showed that mutating S-nitrosylation sites on CSF1R prevented effective inhibition of several pro-tumorigenic markers upon CSF1R inhibition, such as LIF, FGF-9, IL-2, FGF-6, Oncostatin, GDNF, BLC, IFGBP-3, etc. (Fig. 6G). Further, to study if S-nitrosylation of CSF1R is important for GSNO-induced changes in macrophage polarization, we transfected 22RV1 cells with the CSF1R plasmids and exposed the cells to vehicle or GSNO for 48 hours. 22RV1 cells transfected with wild-type CSF1R plasmid only and treated with GSNO demonstrated reduced expression of androgen receptor (AR)(Supplementary Fig. 6) [45]. Together, these results, along with our previous findings [12, 48–50], articulate the potential role of GSNO as a combinatorial partner to augment the anti-tumor effects of CSF1R inhibition against CRPC.

Increased NO levels augment the action of CSF1R inhibition in the suppression of PCa

Next, we tested the impact of combining CSF1Ri with GSNO on LNCAP and 22RV1 cells. Results showed that increasing concentrations of CSF1Ri combined with 50 μM of GSNO concentration significantly decreased cell proliferation in LNCAP cells (Supplementary Fig. 7A). In 22RV1 cells, GSNO had minimal effects on cell

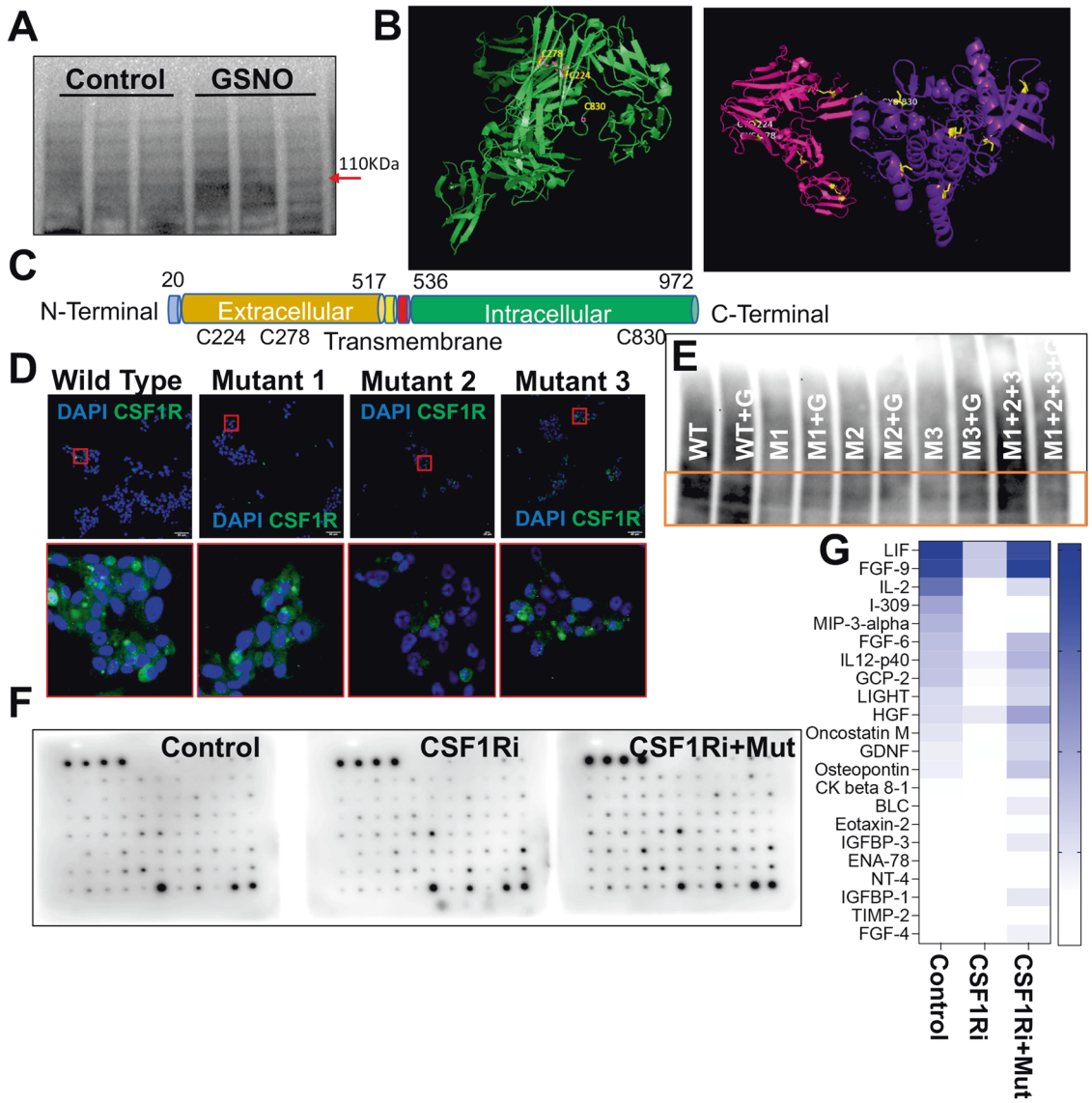

Fig. 6 Increased Nitric oxide induces S-nitrosylation of CSF1R and augments the action of CSF1R inhibition to suppress PCa in vitro. **A** S-nitrosylation in tumor lysates in mice xenografts treated with vehicle (Control) and S-nitrosoglutathione (GSNO) for $n = 3$ samples. **B** A 3D structure of CSF1R showing 3 cysteine sites highlighted in yellow with the highest threshold for nitrosylation. **C** A topology map of CSF1R showing intracellular and extracellular domains and the location of cysteine sites. **D** Representative images show sub-cellular localization of wild-type and three CSF1R mutants (M1, M2, and M3) with deletions at C224, C278, and C830 cysteine residues in 22Rv1 cells. **E** S-nitrosylation in cell lysates in 22Rv1 cell transfected with wild-type mutants with deletion at sites C224, C278, and C830 in the presence/absence of 50 µm S-nitrosoglutathione (GSNO). **F** Cytokine array image of the 22Rv1 cell lysates under different experimental conditions-untreated control, cells treated with CSF1R inhibitor at 0.5 µm dose, and cells transfected with all 3 mutants along with the CSF1Ri. **G** Heat map showing different cytokines differentially expressed in cell lysates treated with CSF1Ri and CSF1R mutants with CSF1Ri. Data are presented as mean ± SEM. $^{***}P < 0.001$; $^{**}P < 0.01$.

proliferation [12](Supplementary Fig. 7B) but increased the inhibitory impact of CSF1Ri on the expression of TMRPSS2 and PSA at RNA (Supplementary Fig. 7C) and AR at protein levels (Supplementary Fig. 7D).

Next, we used U937 cells and treated them with PMA in the presence of pro or anti-inflammatory macrophage-inducing cocktails (Fig. 7A). These cells were then exposed to GSNO (50 µM) and CSF1Ri (0.5 µM) combination (NO-CSF1Ri). Results showed a significant increase in the population of M1 ($CD68^{+}$) and a reduction in M2 ($CD206^{+}CD163^{+}$) macrophages 48 hours post-treatment (Fig. 7A), suggesting that the NO-CSF1Ri combination could effectively inhibit macrophage polarization in-vitro.

Next, we examined the impact of the NO-CSF1Ri combination on reducing the tumor burden of CRPC murine models (castrated C57BL/6 mice, grafted with TRAMP-C2 cells). Treatment conditions included GSNO (10 mg/kg/day IP), CSF1Ri (GW2580, 40 mg/kg/day IP), or combination (GSNO at 10 mg/kg/day + GW2580 at 40 mg/kg/day IP) (Fig. 7B). Importantly, the greatest reduction in tumor burden was achieved in mice receiving the NO-CSF1Ri combination (Fig. 7C) compared to CSF1Ri or GSNO monotherapies. Animals' weight was reduced in the combination and CSF1Ri monotherapy group compared to the control group, unlike mice receiving GSNO alone (Fig. 7C). The tumor grafts from the combination group showed reduced oxidation pockets (Fig. 7D). Moreover, GSNOR activity was reduced by NO-CSF1Ri treatment (Fig. 7E). Additionally, the Griess test on tumor grafts showed that nitrate levels were significantly high ($^{**}p \leq 0.01$) in tumors from the NO-CSF1Ri treatment group (Fig. 7F). This suggests that offsite

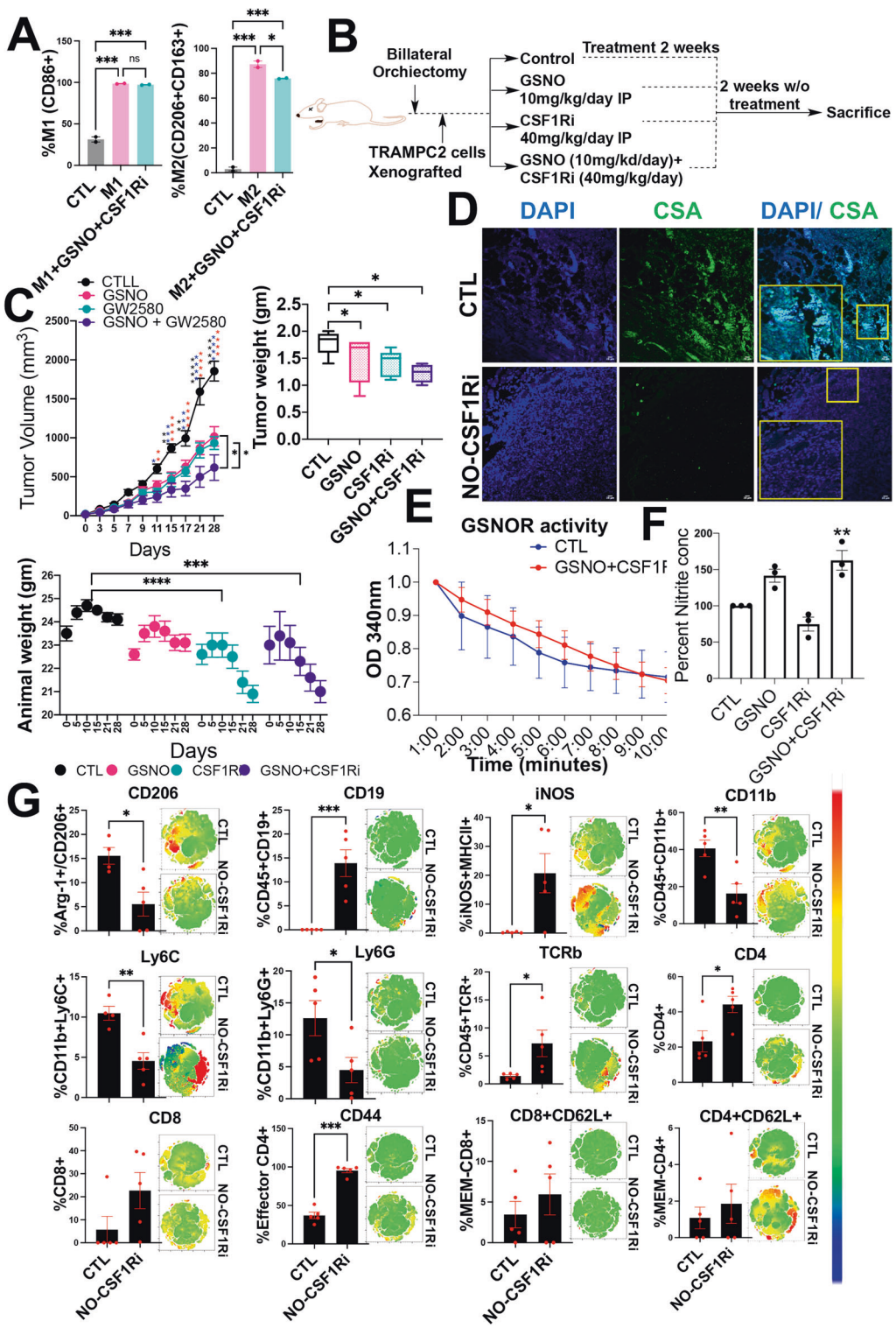

Fig. 7 Impact of NO-CSF1Ri therapy in immune-competent murine models. A Percentage of M1 (CD86+) and M2 (CD206+ CD163+) macrophages in U937 cells used as a model for macrophage differentiation using specific M1 and M2 cocktails when treated in the presence/absence of GSNO + CSF1Ri combination. Data are represented as mean ± SEM. ***$P < 0.001$; **$P < 0.01$, *$P < 0.05$. ns = not significant. **B** Experimental plan. **C** Tumor volume, animal weight, and tumor weight were represented for $n = 5$ animals per treatment condition. **D** Representative immunofluorescent images for tumor sections for mice treated with vehicle and a combination of GSNO and CSF1R inhibitor (NO-CSF1Ri) and stained with 4′,6-diamidino-2-phenylindole (DAPI) (blue), and Cysteine sulfinic acid (red) ($n = 3$). **E** GSNOR activity was measured at 340 nm for 10 minutes using tumor lysates treated with a vehicle and a combination of GSNO and CSF1R inhibitor ($n = 3$). **F** Percent nitrite concentration under different treatment conditions as estimated using the Griess test in tumor lysates ($n = 3$). **G** Immune-phenotyping done in tumor cells in untreated and NO-CSF1Ri mice ($n = 5$) for various markers: CD206, CD19, iNOS, CD11b, Ly6C, Ly6G, TCRB, CD4, CD8, CD44, and CD62L respectively. Data are Mean ± SEM. ***$P < 0.001$; **$P < 0.01$, *$P < 0.05$.

(intraperitoneal) treatment with GSNO as a monotherapy or in combination with CSF1Ri is capable of increasing the nitrite ions in the tumor grafts.

Moreover, NO-CSF1Ri treated mice exhibited reduced expression of AR, ARV7, PSA, TMRPSS2, p-GSK, p-ERK, CD206, KI67, and p90RSK (Supplementary Fig. 7E–G). Furthermore, cytokine array showed, NO-CSF1Ri combination reduced pro-tumorigenic cytokines such as ENA-78, BLC, IP-10, Oncostatin M, FGF-6, IGFBP-3, RANTES, Osteopontin, GCP-2, IL-15, MCP-4, NT-4, TGF- b 3, IL-3, SCF, IL12-p40, IGFBP-4, FGF-4, SDF-1, PDGF-BB, IL-1beta, PARC, TPO, IFN-gamma, FGF-7, and IL-2 (Supplementary Fig. 8A). Next, Immunophenotyping demonstrated that NO-CSF1Ri combination significantly decreased intratumoral percentage of M2 macrophages ($CD45^+CD206^+$), myeloid cells ($CD45^+CD11b^+$), MDSCs ($CD45^+Ly6C^+$), and PMN-MDSCs ($CD45^+Ly6G^+$) and increased the percentage of M1 macrophages ($iNOS^+MHCII^+$), cytotoxic T lymphocytes ($CD8^+$), and effector T cells ($CD44^+CD62L2^-$) (Fig. 7G). Additionally, immunostaining using antibodies against iNOS (M1 macrophage marker), F4/80, and pERK [51], showed that the NO-CSF1Ri combination suppresses the expression of F4/80 and pERK while inducing the expression of iNOS (Supplementary Fig. 8B, C) to reduce macrophage polarization in vivo. Together, these results validate that exogenous supplementation of NO levels augments the action of CSF1Ri to suppress PCa.

DISCUSSION

We observed that NOS3 uncoupling in high-grade human PCa (CRPC) results in a reduction in NO levels and a subsequent increase in oxidative stress, a classic state of nitroso-redox imbalance [25]. The reduced NO level negatively influences the anti-tumor effectiveness of CSF1R blockade therapy as CSF1R at Cys224, Cys278, and Cys830 sites could not be effectively S-nitrosylated. These observations strongly suggested the effectiveness of exogenous NO administration to rebalance the nitroso-redox imbalance and restore CSF1R ability to act against CRPC.

We have previously shown that increased levels of NO are associated with lowering luteinizing hormone and testosterone [50], suggesting the tumor inhibitory role of NO against PCa [12, 52]. Here, our studies show the following findings—(a) uncoupled NOS3 increases the overall oxidative stress in high-grade PCa; (b) diminished S-nitrosylation of three cysteine residues reduces the anti-tumor abilities of CSF1R blockade; (c) exogenous NO treatment S-nitrosylates CSF1R at Cys224, Cys278, and Cys830 sites; (d) in the presence of exogenous NO, CSF1Ri blockade can effectively reduce CRPC tumor burden, compared to NO or CSF1R blockade monotherapies; (e) the intratumor percentage of M2 macrophages ($CD45^+F4/80^+$, $CD206^+$), $CD45^+Ly6G^+$, and $CD45^+Ly6C^+$, $CD45^+CD11b^+$ cells are decreased, and that of M1 macrophages ($iNOS^+MHCII^+$), cytotoxic T lymphocytes ($CD8^+$), effector T cells ($CD44^+CD62L^-$), B cells ($CD45^+CD19^+$) are increased upon NO-CSF1R blockade; (e) several pro-tumorigenic cytokines which are not effectively reduced by CSF1Ri monotherapy are reduced upon NO-CSF1R blockade. Together the results suggested that an exogenous increase in NO could increase the efficacy of CSF1R blockade against CRPC

Our study has limitations that should be addressed with further work. For example, 1. though we tested different combinations of GSNO and CSF1Ri in vitro, the correlation between concentrations of NO-CSF1Ri and in-vivo tumor burden reduction remains unexplored. 2. We showed that S-nitrosylation of three different cystines on CSF1R molecule via GSNO is important to modulate inhibitory effects on CRPC tumors, however, what other molecules are S-nitrosylated and how they could modulate NO-CSF1R blockade therapy still needs to be explored. We showed earlier that increased NO levels are capable of affecting hypogonadism [50] and leading to CRPC tumor suppression, which therefore leads to the possibility that tumor inhibition could be profound in non-castrate mice. However, this assumption requires future exploration.

In conclusion, our findings offer insights into an under-explored area of CRPC therapeutics. The mechanistic insights gathered in this study provide a strong rationale for initiating in vivo experiments with possible advancement into clinical trials with NO-CSF1R blockade in patients with advanced metastatic stages of cancer.

DATA AVAILABILITY

All data, codes, and materials used in the study are available to any researcher for reproducing or extending the analysis. Materials transfer agreements (MTAs) will be required to request access. RNA sequencing data have been deposited in a public database.

REFERENCES

1. Torre LA, Bray F, Siegel RL, Ferlay J, Lortet-Tieulent J, Jemal A. Global cancer statistics, 2012. CA Cancer J Clin. 2015;65:87–108.
2. Escamilla J, Schokrpur S, Liu C, Priceman SJ, Moughon D, Jiang Z, et al. CSF1 receptor targeting in prostate cancer reverses macrophage-mediated resistance to androgen blockade therapy. Cancer Res. 2015;75:950–62.
3. Hotte SJ, Saad F. Current management of castrate-resistant prostate cancer. Curr Oncol. 2010;17:S72–79.
4. James ND, Sydes MR, Clarke NW, Mason MD, Dearnaley DP, Spears MR, et al. Addition of docetaxel, zoledronic acid, or both to first-line long-term hormone therapy in prostate cancer (STAMPEDE): survival results from an adaptive, multi-arm, multistage, platform randomised controlled trial. Lancet. 2016;387:1163–77.
5. James ND, de Bono JS, Spears MR, Clarke NW, Mason MD, Dearnaley DP, et al. Abiraterone for Prostate Cancer Not Previously Treated with Hormone Therapy. N. Engl J Med. 2017;377:338–51.
6. Hench IB, Cathomas R, Costa L, Fischer N, Gillessen S, Hench J. et al. Analysis of AR/ARV7 Expression in Isolated Circulating Tumor Cells of Patients with Metastatic Castration-Resistant Prostate Cancer (SAKK 08/14 IMPROVE Trial). Cancers. 2019;11:1099.
7. Balkwill FR, Capasso M, Hagemann T. The tumor microenvironment at a glance. J Cell Sci. 2012;125:5591–6. Pt 23
8. Poh AR, Ernst M. Targeting Macrophages in Cancer: From Bench to Bedside. Front Oncol. 2018;8:49.
9. Noy R, Pollard JW. Tumor-associated macrophages: from mechanisms to therapy. Immunity. 2014;41:49–61.
10. De Palma M, Lewis CE. Macrophage regulation of tumor responses to anticancer therapies. Cancer Cell. 2013;23:277–86.
11. Hamilton JA. Colony-stimulating factors in inflammation and autoimmunity. Nat Rev Immunol. 2008;8:533–44.
12. Arora H, Panara K, Kuchakulla M, Kulandavelu S, Burnstein KL, Schally AV, et al. Alterations of tumor microenvironment by nitric oxide impedes castration-resistant prostate cancer growth. Proc Natl Acad Sci USA. 2018;115:11298–303.
13. Benner B, Good L, Quiroga D, Schultz TE, Kassem M, Carson WE, et al. Pexidartinib, a Novel Small Molecule CSF-1R Inhibitor in Use for Tenosynovial Giant Cell Tumor: A Systematic Review of Pre-Clinical and Clinical Development. Drug Des Devel Ther. 2020;14:1693–704.
14. Cannarile MA, Weisser M, Jacob W, Jegg AM, Ries CH, Ruttinger D. Colony-stimulating factor 1 receptor (CSF1R) inhibitors in cancer therapy. J Immunother Cancer. 2017;5:53.
15. Mao Y, Eissler N, Blanc KL, Johnsen JI, Kogner P, Kiessling R. Targeting Suppressive Myeloid Cells Potentiates Checkpoint Inhibitors to Control Spontaneous Neuroblastoma. Clin Cancer Res. 2016;22:3849–59.
16. Neubert NJ, Schmittnaegel M, Bordry N, Nassiri S, Wald N, Martignier C. et al. T cell-induced CSF1 promotes melanoma resistance to PD1 blockade. Sci Transl Med. 2018;10:eaan3311.
17. Garcia-Ortiz A, Serrador JM. Nitric Oxide Signaling in T Cell-Mediated Immunity. Trends Mol Med. 2018;24:412–27.
18. Alderton WK, Cooper CE, Knowles RG. Nitric oxide synthases: structure, function and inhibition. Biochem J. 2001;357:593–615. Pt 3
19. Zimmet JM, Hare JM. Nitroso-redox interactions in the cardiovascular system. Circulation. 2006;114:1531–44.
20. Barouch LA, Harrison RW, Skaf MW, Rosas GO, Cappola TP, Kobeissi ZA, et al. Nitric oxide regulates the heart by spatial confinement of nitric oxide synthase isoforms. Nature. 2002;416:337–9.

21. Lee WJ, Tateya S, Cheng AM, Rizzo-DeLeon N, Wang NF, Handa P, et al. M2 Macrophage Polarization Mediates Anti-inflammatory Effects of Endothelial Nitric Oxide Signaling. Diabetes. 2015;64:2836–46.
22. Benhar M. Emerging Roles of Protein S-Nitrosylation in Macrophages and Cancer Cells. Curr Med Chem. 2016;23:2602–17.
23. Stomberski CT, Hess DT, Stamler JS. Protein S-Nitrosylation: Determinants of Specificity and Enzymatic Regulation of S-Nitrosothiol-Based Signaling. Antioxid Redox Signal. 2019;30:1331–51.
24. Rabender CS, Alam A, Sundaresan G, Cardnell RJ, Yakovlev VA, Mukhopadhyay ND, et al. The Role of Nitric Oxide Synthase Uncoupling in Tumor Progression. Mol Cancer Res. 2015;13:1034–43.
25. Hare JM. Nitroso-redox balance in the cardiovascular system. N. Engl J Med. 2004;351:2112–4.
26. Hare JM, Stamler JS. NO/redox disequilibrium in the failing heart and cardiovascular system. J Clin Investig. 2005;115:509–17.
27. Blanchette J, Jaramillo M, Olivier M. Signalling events involved in interferon-gamma-inducible macrophage nitric oxide generation. Immunology. 2003;108:513–22.
28. Fonseca SG, Romao PR, Figueiredo F, Morais RH, Lima HC, Ferreira SH, et al. TNF-alpha mediates the induction of nitric oxide synthase in macrophages but not in neutrophils in experimental cutaneous leishmaniasis. Eur J Immunol. 2003;33:2297–306.
29. Beigi F, Gonzalez DR, Minhas KM, Sun QA, Foster MW, Khan SA, et al. Dynamic denitrosylation via S-nitrosoglutathione reductase regulates cardiovascular function. Proc Natl Acad Sci USA. 2012;109:4314–9.
30. Gonzalez DR, Treuer AV, Castellanos J, Dulce RA, Hare JM. Impaired S-nitrosylation of the ryanodine receptor caused by xanthine oxidase activity contributes to calcium leak in heart failure. J Biol Chem. 2010;285:28938–45.
31. Kulandavelu S, Dulce RA, Murray CI, Bellio MA, Fritsch J, Kanashiro-Takeuchi R, et al. S-Nitrosoglutathione Reductase Deficiency Causes Aberrant Placental S-Nitrosylation and Preeclampsia. J Am Heart Assoc. 2022;11:e024008.
32. Barca C, Foray C, Hermann S, Herrlinger U, Remory I, Laoui D, et al. The Colony Stimulating Factor-1 Receptor (CSF-1R)-Mediated Regulation of Microglia/Macrophages as a Target for Neurological Disorders (Glioma, Stroke). Front Immunol. 2021;12:787307.
33. Chitu V, Gokhan S, Nandi S, Mehler MF, Stanley ER. Emerging Roles for CSF-1 Receptor and its Ligands in the Nervous System. Trends Neurosci. 2016;39:378–93.
34. Stanley ER, Chitu V. CSF-1 receptor signaling in myeloid cells. Cold Spring Harb Perspect Biol. 2014;6:a021857.
35. Lin JZ, Wang WW, Hu TT, Zhu GY, Li LN, Zhang CY, et al. FOXM1 contributes to docetaxel resistance in castration-resistant prostate cancer by inducing AMPK/mTOR-mediated autophagy. Cancer Lett. 2020;469:481–9.
36. Goncalves DA, Jasiulionis MG, Melo FHM. The Role of the BH4 Cofactor in Nitric Oxide Synthase Activity and Cancer Progression: Two Sides of the Same Coin. Int J Mol Sci. 2021;22:9546.
37. Barnett SD, Buxton ILO. The role of S-nitrosoglutathione reductase (GSNOR) in human disease and therapy. Crit Rev Biochem Mol Biol. 2017;52:340–54.
38. Werner ER, Gorren AC, Heller R, Werner-Felmayer G, Mayer B. Tetrahydrobiopterin and nitric oxide: mechanistic and pharmacological aspects. Exp Biol Med. 2003;228:1291–302.
39. Berka V, Yeh HC, Gao D, Kiran F, Tsai AL. Redox function of tetrahydrobiopterin and effect of L-arginine on oxygen binding in endothelial nitric oxide synthase. Biochemistry. 2004;43:13137–48.
40. Beffinger M, Tallon de Lara P, Tugues S, Vermeer M, Montagnolo Y, Ohs I, et al. CSF1R-dependent myeloid cells arerequired for NKmediated control of metastasis. JCI Insight. 2018;3:e97792.
41. Mahajan N, Shi HY, Lukas TJ, Zhang M. Tumor-suppressive maspin functions as a reactive oxygen species scavenger: importance of cysteine residues. J Biol Chem. 2013;288:11611–20.
42. Seo YH, Carroll KS. Profiling protein thiol oxidation in tumor cells using sulfenic acid-specific antibodies. Proc Natl Acad Sci USA. 2009;106:16163–8.
43. Erlandsson A, Carlsson J, Lundholm M, Falt A, Andersson SO, Andren O, et al. M2 macrophages and regulatory T cells in lethal prostate cancer. Prostate. 2019;79:363–9.
44. Zhu W, Zhao Z, Chou F, Zuo L, Liu T, Yeh S, et al. Loss of the androgen receptor suppresses intrarenal calcium oxalate crystals deposition via altering macrophage recruitment/M2 polarization with change of the miR-185-5p/CSF-1 signals. Cell Death Dis. 2019;10:275.
45. Becerra-Diaz M, Strickland AB, Keselman A, Heller NM. Androgen and Androgen Receptor as Enhancers of M2 Macrophage Polarization in Allergic Lung Inflammation. J Immunol. 2018;201:2923–33.
46. Cioni B, Zaalberg A, van Beijnum JR, Melis MHM, van Burgsteden J, Muraro MJ, et al. Androgen receptor signalling in macrophages promotes TREM-1-mediated prostate cancer cell line migration and invasion. Nat Commun. 2020;11:4498.
47. Nelson EJ, Connolly J, McArthur P. Nitric oxide and S-nitrosylation: excitotoxic and cell signaling mechanism. Biol Cell. 2003;95:3–8.
48. Mintz J, Vedenko A, Rosete O, Shah K, Goldstein G, Hare JM. et al. Current Advances of Nitric Oxide in Cancer and Anticancer Therapeutics. Vaccines. 2021;9:94.
49. Vedenko A, Panara K, Goldstein G, Ramasamy R, Arora H. Tumor Microenvironment and Nitric Oxide: Concepts and Mechanisms. Adv Exp Med Biol. 2020;1277:143–58.
50. Masterson TA, Arora H, Kulandavelu S, Carroll RS, Kaiser UB, Gultekin SH, et al. S-Nitrosoglutathione Reductase (GSNOR) Deficiency Results in Secondary Hypogonadism. J Sex Med. 2018;15:654–61.
51. Richardson ET, Shukla S, Nagy N, Boom WH, Beck RC, Zhou L, et al. ERK Signaling Is Essential for Macrophage Development. PLoS One. 2015;10:e0140064.
52. Soni Y, Softness K, Arora H, Ramasamy R. The Yin Yang Role of Nitric Oxide in Prostate Cancer. Am J Mens Health. 2020;14:1557988320903191.

ACKNOWLEDGEMENTS

We thank all the mentors (Dr. Dipen J Parekh), collaborators (Dr. Bonnie Bloomberg), graduate student (Anastasia Vedenko), and Postdoctoral students (Dr. Deepa Seetharam) for their insights, suggestions, and support during this study.

AUTHOR CONTRIBUTIONS

HA, and FF performed most experiments with the assistance of MK, RQ, YS, KS, RAD, and TM. HA conceived the project and designed the experiments. HA and JMH analyzed and interpreted the data. DVB performed the bioinformatic analysis. HA, RR, JMH, and RQ wrote the manuscript. All authors had the opportunity to discuss the results and comment on the manuscript.

COMPETING INTERESTS

Authors declare that they have no competing interests. JMH reports having a patent for cardiac cell-based therapy and holds equity in Vestion Inc., and maintains a professional relationship with Vestion Inc. as a consultant and member of the Board of Directors and Scientific Advisory Board. Vestion Inc. did not play a role in the design, conduct, or funding of the study. JMH is the Chief Scientific Officer, a compensated consultant, and a board member for Longeveron Inc. and holds equity in Longeveron. JMH is also the co-inventor of intellectual property licensed to Longeveron. Longeveron did not play a role in the design, conduct, or funding of the study. The University of Miami is an equity owner in Longeveron Inc., which has licensed intellectual property from the University of Miami.

ADDITIONAL INFORMATION

Supplementary information The online version contains supplementary material available at https://doi.org/10.1038/s41419-022-05289-4.

Correspondence and requests for materials should be addressed to Himanshu Arora.

Reprints and permission information is available at http://www.nature.com/reprints

Publisher's note Springer Nature remains neutral with regard to jurisdictional claims in published maps and institutional affiliations.